Engineering Structures 316 (2024) 118551

Contents lists available at ScienceDirect

Engineering Structures

journal homepage: www.elsevier.com/locate/engstruct

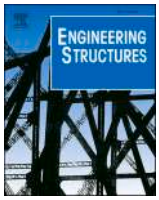

Hybrid simulation of steel frames with Dissipative Replaceable Link Frame and high-strength steel coupling beams

Giulia Giuliani [1], Roberto Andreotti [2], Alessio Bonelli [3], Nicola Tondini [*,4]

University of Trento - Department of Civil, Environmental and Mechanical Engineering, Via Mesiano 77, 38123 Trento, Italy

ARTICLE INFO

Keywords:
Full-scale experimental tests
Hybrid simulation
Steel structures
Seismic devices
Resilient structures
Repairability
High strength steel
Coupling beams

ABSTRACT

The paper describes the results of an experimental campaign conducted on full-scale steel frames equipped with dissipative components within the European Research Fund for Coal and Steel (RFCS) pilot project DISSIPABLE. Dissipative Replaceable Link Frame (DRLF), whose characteristic is the large energy dissipation combined with ease of replacement, were installed on the frame and coupled through high-strength steel (HSS) beams characterised by an elastic response to increase the overall frame stiffness and to improve the re-centring capability after a major seismic event. The seismic performance of the steel frame was investigated by means of Hybrid Simulation (HS) at three different limit states, i.e., damage limitation (DL), significant damage (SD) and near collapse (NC). In particular, the first floor of the frame was physically built, whilst the response of the remaining five floors was numerically simulated. The results of the tests highlighted the large dissipation capabilities of the DRLF system. In addition, the high-strength steel coupling beams remained elastic even at the NC limit state and provided excellent behaviour in increasing stiffness and re-centring capabilities. Finally, the repairability of the DRLF components was demonstrated.

1. Introduction

Unpredictable natural disasters like earthquakes have devastating consequences for the environment and communities, often resulting in the collapse of buildings, significant economic losses, and casualties. Current building design codes and guidelines [1–3] rely on energy dissipation mechanisms and capacity design principles to enable buildings to withstand seismic actions. For example, in moment resisting frames (MRF), plastic hinges are formed at the ends of beams. Various approaches, like reduced beam sections (RBSs) at the element ends, have been explored to facilitate high dissipative behaviour [4,5]. Furthermore, research has explored the use of partial-strength joints in place of the traditional full-strength connections between beams and columns [6,7] as well as column bases [8,9] to concentrate energy dissipation [10–16] or by adding dampers to the joints [15,16]. While effective in protecting lives under seismic loading, those solutions do not guarantee rapid post-earthquake repairs, leading to extended downtime and economic losses.

In response, researchers have focused on energy dissipation solutions that are able to enhance structural resilience and are replaceable and affordable. Friction connections were investigated since they allow for the dissipation of large amounts of energy without experiencing high damage [17–21]. Slit dampers have been experimentally tested for eccentrically braced frames [22] and moment resisting frames [23], exhibiting a wide and compact hysteretic behaviour in both cases. Those results demonstrated that the slit dampers effectively dissipate energy and provide the desired damping characteristics. Added Damping and Stiffness (ADAS and TADAS) dampers [24], have also been investigated. These dampers have shown suitable hysteretic behaviour when subjected to natural ground acceleration records, effectively providing additional damping to the structure while preserving the integrity of the main elements. Linked Column Frame (LCF) systems, consisting in steel columns connected by replaceable link that act like fuses, were studied in [25–30]. These studies demonstrated the effectiveness of such solutions in dissipating energy and protecting the main structure from damage. However, there is a lack of experimental tests on full-scale

* Corresponding author.
E-mail address: nicola.tondini@unitn.it (N. Tondini).
[1] ORCID: 0000-0002-7085-6408
[2] ORCID: 0000-0001-6895-9152
[3] ORCID: 0000-0003-2398-9432
[4] ORCID: 0000-0003-2602-6121

https://doi.org/10.1016/j.engstruct.2024.118551
Received 25 January 2024; Received in revised form 29 May 2024; Accepted 1 July 2024
Available online 20 July 2024

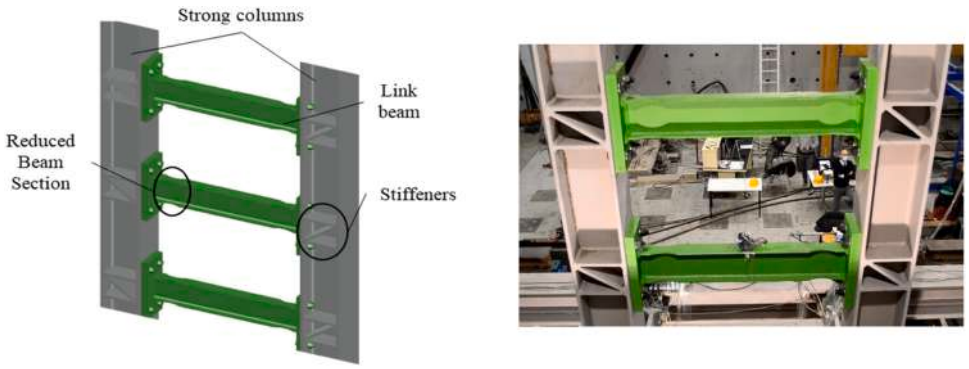

Fig. 1. DRLF system configuration.

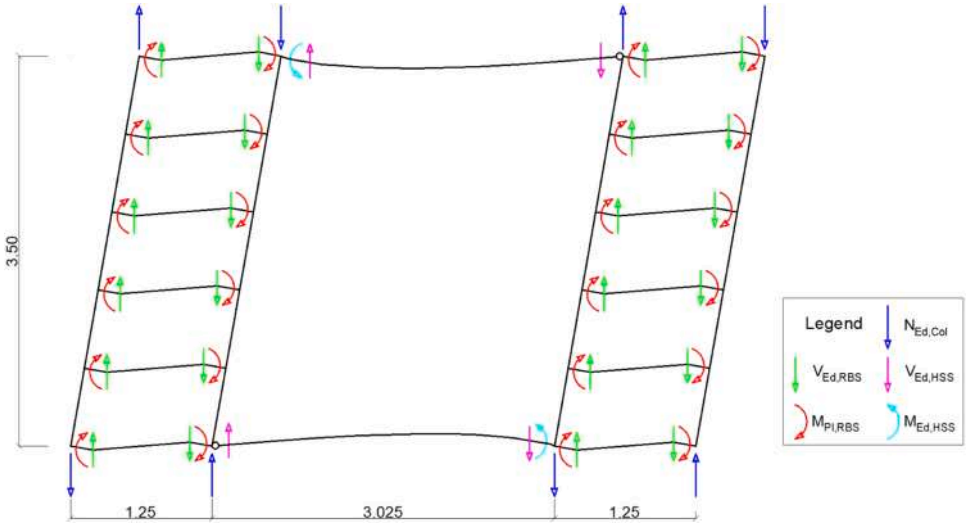

Fig. 2. Lateral-resisting mechanism. Dimension in meters.

frames, and no investigations have been conducted on the actual replaceability of beam links. These solutions has also been proven effective as a retrofit measure, as demonstrated by Ezodin et al. [31].

In order to ensure that buildings incur minimal damage and thus enhance their structural resilience, a viable strategy is to provide structures with self-centring capabilities [32]. Moreover, the partial self-centring behaviour of structures also offers advantages in terms of life-cycle costs [33]. Various approaches are available to achieve partial or full self-centring proficiency. For instance, Self-Centring Column Bases [34], designed for application in a steel moment resisting frame, have proven highly effective in minimising structural residual displacement.

On these premises, in recent years, the scientific community has focused on developing systems able to guarantee the dissipation of the seismic action and that could be easily replaced if damaged, reducing the material consumption and costs related to serviceability restoration. In this context, a series of European projects were carried out. In particular, the INERD project [35] and the FUSEIS project [36] conceptualised the design. They investigated the seismic behaviour of innovative devices capable of dissipating significant energy and being replaced after a seismic event. In greater detail, the INERD project dealt with energy dissipation in bracing systems [37], whilst in the FUSEIS projects, major attention was given to moment resisting frames by conceiving two different devices, namely FUSEIS 1 [38,39] and FUSEIS 2 [40]. More recently, the DISSIPABLE [41] pilot project was funded to provide experimental evidence on typical steel and composite steel-concrete frame in terms of energy dissipation and ease of reparability after a major seismic event. Three different components were examined, namely Dissipative Replaceable Braced Connections (DRBrC) [42], Dissipative Replaceable Link Frame (DRLF) and Dissipative Replaceable Beam Splices (DRBeS) [43], which were respectively named in the previous projects as INERD, FUSEIS type 1 and FUSEIS type 2. The experimental campaign conducted at the University of Trento on the DRLF system successfully bridged the gap between previous RFCS projects, where only tests on the single components were carried out, by performing full-scale tests on frames equipped with dissipative components. The experimental test results demonstrated the component's ability to dissipate energy and protect critical and irreplaceable elements of the structures. Furthermore, the repairability of the structure after an intense seismic event was also verified. Two distinct sets of tests were conducted on frames equipped with the DRLF system. In the first set, the favourable dissipative behaviour of the DRLF system was demonstrated when employed in an entirely mild-steel structure [44]. The experimental outcomes of these tests were employed to calibrate the non-linear numerical models of the RBSs, which were extensively used in the presented work. Furthermore, the paper examines the potential advantages of utilizing coupling beams made of HSS to enhance the structure resilience and increase the frame stiffness, as proposed in [45–47]. For that purpose, a six-storey frame with alternatively fixed HSS beams in the non-dissipative zones was subjected to investigation. HSS coupling beams were employed to ensure that the frame remains elastic even during high-intensity seismic events. In previous years, several studies have been carried out to evaluate the use of HSS in steel or steel-concrete composite structures for

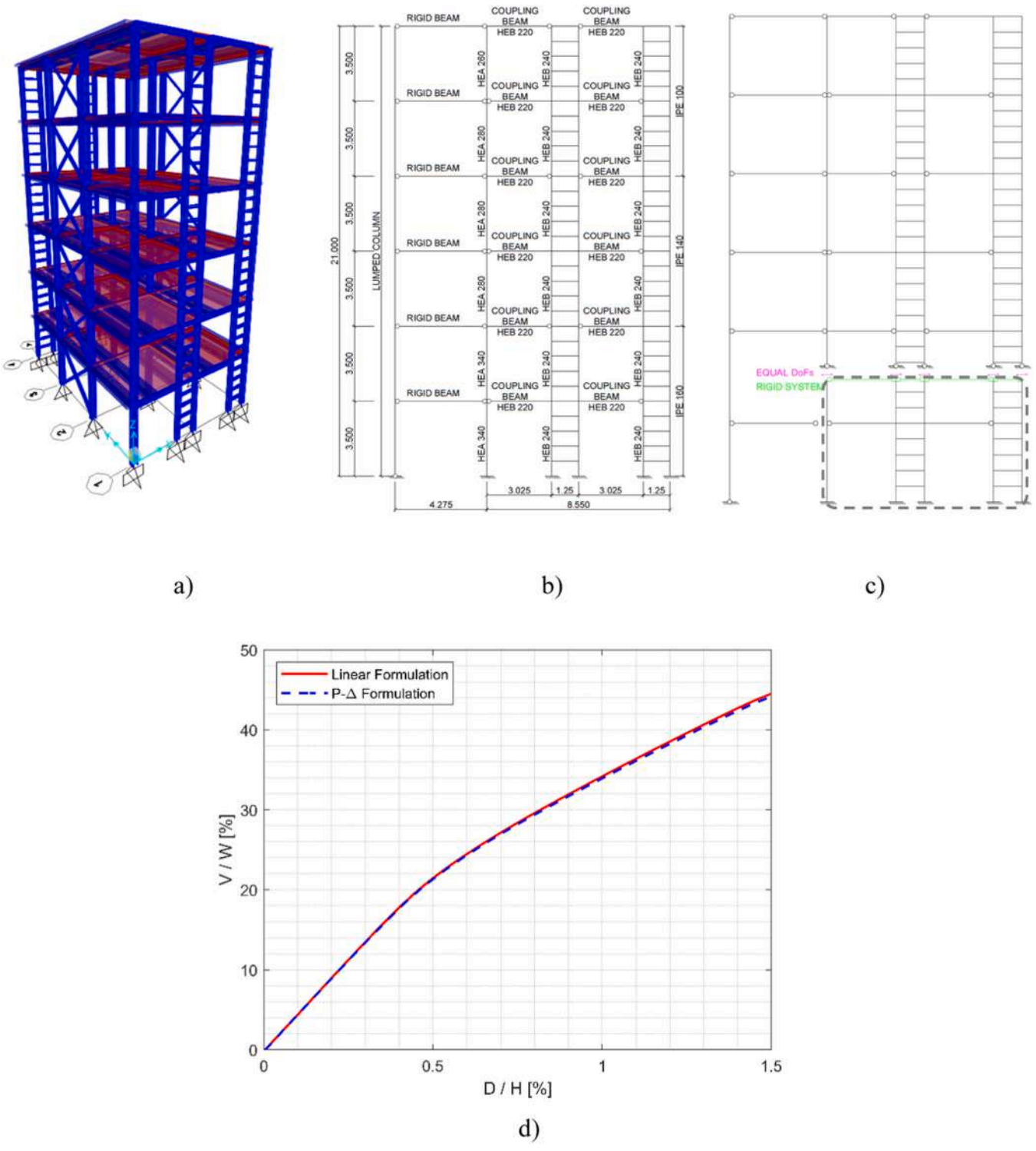

Fig. 3. Substructuring of the prototype building: a) 3D Building; b) 2D Frame; c) Substructured Frame; d) Influence of P-Δ effect on the substructured frame.

both dissipative [48] and non-dissipative elements [49,50]. The Hybrid Simulation (HS) technique was exploited, enabling full-scale frames to be tested by physically building only part of the structure, whilst numerically simulating the remainder. HS for experimental tests in civil engineering was proposed in the early '70 [51] and has been successfully applied and validated since then [52–54]. The paper is organised as follows: a brief description of the dissipative component under investigation is given in Section 2; in Section 3, the description of the numerical model implemented for the simulation is described, whilst the basic concepts of the HS procedure employed in the tests are presented in Section 4 together with the laboratory mock-up. Section 5 describes the test programme as well as the ground motion selection, while Section 5.2 reports the experimental test results. Finally, in Section 5.3, the conclusive remarks are drawn.

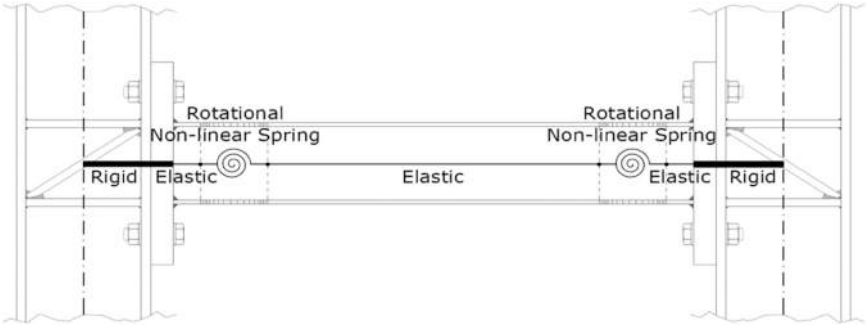

Fig. 4. Beam link numerical model.

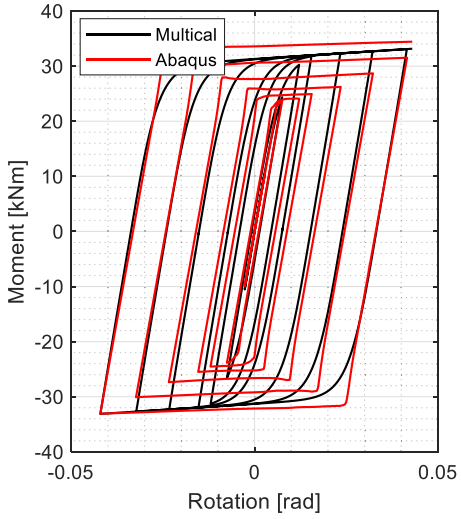

Fig. 5. RBS cyclic behaviour of the IPE160 profile.

2. Dissipative Replaceable Link Frame (DRLF) system and coupling beams

The Dissipative Replaceable Link Frame (see Fig. 1) is composed of two rigid, closely spaced columns connected by multiple beams through bolted connections. The beam links may work mainly in bending or shear, based on their length, whilst the columns are subjected to a strong axial force [55]. By weakening the beam links at their ends, the plastic hinges are induced at those locations, i.e. the RBSs, designed in accordance with Eurocode 8–3 [56]. Moreover, the beam links are not part of the gravity load-carrying system, ensuring easy replaceability after a major seismic event. In general, when connecting the DRLF with coupling beams, the overall frame develops two lateral-resisting schemes. The DRLF contributes to global strength, stiffness and energy dissipation, whilst the additional frame, consisting of the strong columns and the coupling beams, adds further strength and stiffness to reduce the deformability and enhance the structure repairability [45–47]. Once the DRLF undergoes large inelastic behaviour, its contribution to the overall stiffness decreases, and, consequently, the force demand in the coupling beams increases. Thus, the coupling beams must be designed with overstrength to withstand the additional loading after the beam links yield. For this reason, the coupling beams are made of high-strength steel, and a steel grade S460 was chosen in this work. Moreover, after carrying out a set of numerical studies, a pinned-fixed joint solution was selected for the coupling beams as the optimal configuration for guaranteeing a substantial stiffness contribution as well as avoiding the premature yielding of such elements. Fig. 2 depicts the described lateral-resisting mechanism.

3. Design of the prototype structure

To analyse the seismic performance of the DRLF system coupled with the HSS beams, a prototype six-storey building was designed according to the Eurocodes (see Fig. 3). In greater detail, a 3D linear model was subjected to dynamic analysis with response spectrum, characterised by peak ground acceleration (PGA) equal to 0.36 g at the Significant Damage (SD) limit state and soil type A. In this respect, a 3D finite element (FE) model was developed in SAP2000 [57]. The building has an inter-storey height of 3.5 m, and a span length of 4.275 m, which was determined to fit the geometrical laboratory constraints. The structure had two and three spans in the main directions, respectively, whilst the laterally resisting frames were located along the structure perimeter. The frame composed by the DRLF component and the coupling beams was located in the two-span directions, whilst a concentrically braced frame (CBF) equipped with the DRBrC component [42,58] was located in the three-span direction. The study examined the use of HSS, namely S460 steel grade, for the coupling beams due to their high seismic strength demand, which is required to couple two DRLF. Additionally, once the beam links undergo plastic deformation, the contribution of the coupling beams to the overall stiffness increases, further augmenting their load demand. Concerning the other elements, S355 steel grade was chosen for the non-dissipative members, whilst for the dissipative beam links, i.e. the IPE profiles that constitute the DRLF, an S235 steel grade was employed. Member profiles and component dimensions are depicted in Fig. 3b. The dissipative components were designed according to Eurocode 8–3 [56], whilst the non-dissipative elements were checked referring to Eurocode 8–1 [1] and the INNOSEIS provisions [55]. Moreover, the static design was performed by following Eurocode 3–1-1 [59] provisions. To investigate the non-linear behaviour, a reference 3D model was developed in the FE software OpenSees [60]. Beams and columns were modelled by means of “ElasticBeamColumn” elements, whilst the beam links were subdivided into five segments, as shown in Fig. 4 [55]. The non-linear elements, i.e., the RBSs, were modelled employing a “TwoNodeLink” element while the remaining parts were modelled as “ElasticBeamColumns” elements with the mechanical properties of the gross section. A rigid link was inserted at both ends of the beam to reproduce the moment-resisting joint between the beams and the column and avoid considering additional flexibility. The Bouc–Wen [61] model was chosen for the rotational degree of freedom (DoF) of the “TwoNodeLink” element as it was the most suitable to reproduce the hysteretic behaviour of the steel sections. An initial estimation was based on a RBS model developed in the finite element software ABAQUS [62], see Fig. 5. In a second stage, the Bouc-Wen model parameters were calibrated on the results of previous tests conducted at the University of Trento on a different structure entirely made of mild steel and equipped with the DRLF system [41,44,63].

Since the tests were performed on a 2D frame, it was necessary to develop a 2D FE model that reproduced the behaviour of the building well in the DRLF direction. To take the gravity frames into account, a

Table 1
Modal comparison between 3D building, 2D frame and 2D SF.

Mode	3D Periods [s]	2D Periods [s]	2D SF Periods [s]	Error 3 D–2D	Error 2D-SF
1	1.33	1.26	1.21	5 %	4 %
2	0.42	0.41	0.42	1 %	1 %
3	0.21	0.21	0.22	0 %	1 %

Table 2
MAC matrix between 3D Building and 2D Frame.

		2D Frame		
	Mode	**1**	**2**	**3**
3D Building	**1**	1	0	0
	4	0	1	0
	8	0	0	1

Table 3
MAC matrix between 2D Frame and 2D SF.

		2D SF		
	Mode	1	2	3
2D Frame	**1**	1	0	0
	2	0	0.99	0
	3	0	0	1

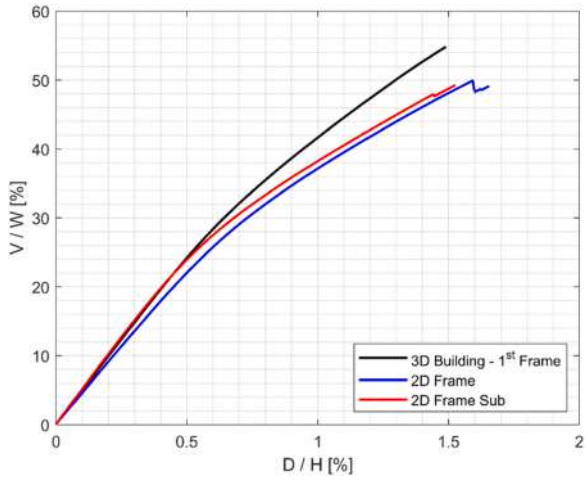

Fig. 6. Pushover comparison.

lumped column [64] was introduced in the 2D model. Given the three spans in the CBF direction, two internal gravity frames were oriented in the DRLF direction. Therefore, the lumped column modulus of inertia was calculated floor by floor as the sum of the modulus of inertia of the columns associated with one internal gravity frame. Indeed, half of the total mass was assigned to the frame and concentrated in one node on each floor, placed at the top of the central column and connected to the others by means of rigid links. The 2D model is depicted in Fig. 3b. To exploit hybrid simulation, the substructuring technique was employed. Since only two translational DoFs can be controlled in the laboratory, the procedure to define the substructured configuration led to subdivide the structure at the midpoint of the second-floor columns, which well approximates the position of the inflection point, as shown in Fig. 3c. In doing so, by controlling the horizontal DoFs located at the first floor and at mid-height of the second floor, the structural seismic behaviour could be effectively reproduced in the laboratory. To give continuity between the two subdomains, horizontal constraints were introduced at the interface between the two subdomains, so that the displacement applied at the top of the physical subdomain columns was the same as the base of the numerical subdomain. In addition, vertical restraints were imposed at the base of the numerical subdomain to avoid an ill-conditioned problem, i.e., a floating domain in the vertical direction. The influence of these simplifications on the structural behaviour was investigated by comparing the response of the three levels of modelling, namely 3D building, 2D frame and 2D Substructured Frame (SF), in terms of modal analysis. The consistency of the periods and the vibration modes according to Modal Assurance Criterion (MAC) [65] was checked, as reported in Tables 1-3 . Furthermore, a thorough investigation was conducted on the P-Δ effects, see Fig. 3d, which revealed that second order effects did not significantly influence the overall structural behaviour of the substructured frame. Consequently, the application of the vertical axial load on the physical substructure was avoided. Furthermore, the non-linear behaviour was compared by means of pushover analysis, and the corresponding results are presented in Fig. 6. The outcomes showed a very good agreement between the three different modelling levels, with errors within 10 %.

To perform hybrid simulations with a reasonable computational demand, a limited DoFs number of the numerical subdomain was required; hence, two condensation steps were followed. First, the beam link model depicted in Fig. 4 was condensed into a shear spring, modelled in OpenSees [60] as shown in Fig. 7. The non-linear parameters were calibrated based on the results of numerical analyses performed on the single beam links.

Second, the five shear springs of each floor were further condensed into one, as depicted in Fig. 8. To calibrate the related Bouc-Wen parameters, a displacement control analysis was performed by imposing a cyclic displacement at the top floor of the reference model. The results of the pushover and time-history analyses at the NC limit state on the three structures are depicted in Figs. 9 and 10, highlighting a good agreement between the models.

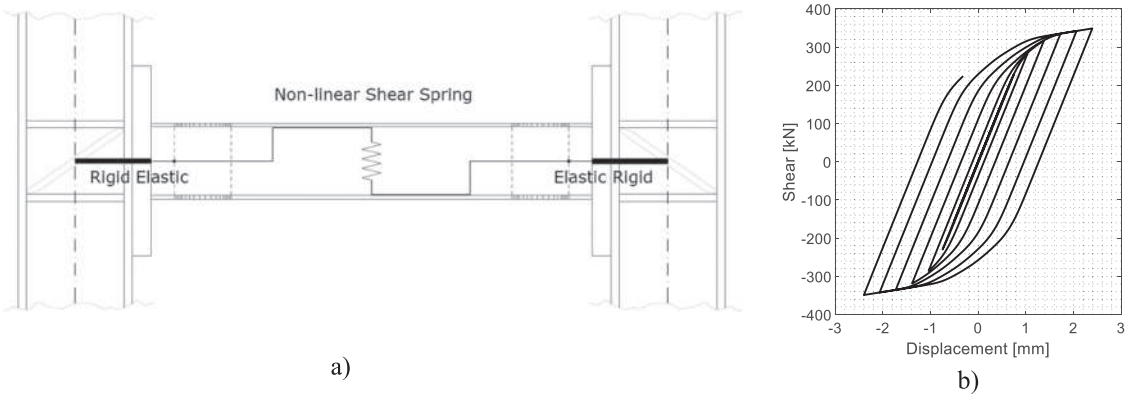

a) b)

Fig. 7. a) Condensed beam link model; b) RBS numerical modelling in OpenSees of the IPE160 profile.

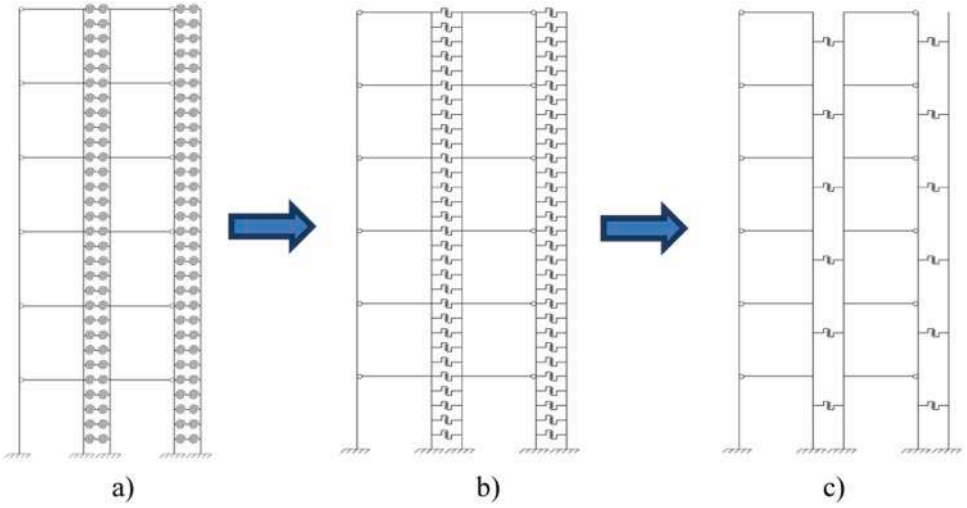

Fig. 8. Reduced models: a) reference model, b) condensed beam link model and c) condensed model.

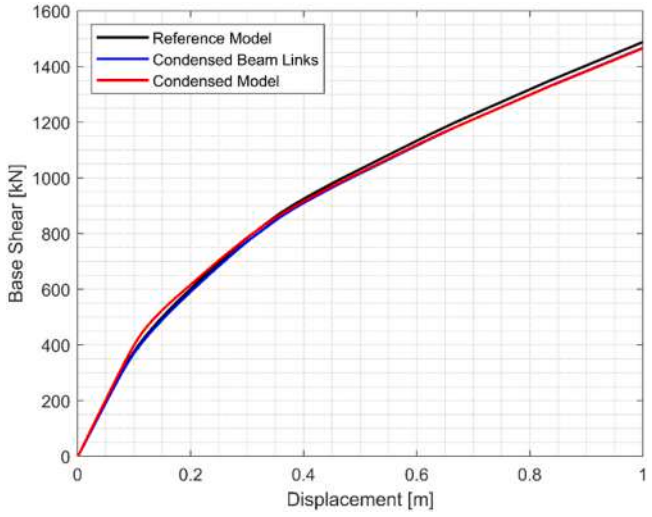

Fig. 9. Pushover comparison between reference and condensed models.

4. Hybrid simulation

4.1. Hybrid simulation algorithm

The experimental campaign was carried out through HS technique, where the full-scale substructure of the ground floor was built up in the laboratory and tested by means of hydraulic actuators, whilst the remaining part was numerically simulated. The physical and numerical substructure's response, PS and NS, is computed and coupled step-by-step by the partitioned G-α algorithm [66]. In particular, Lagrange multipliers were employed, representing the interface forces exchanged between NS and PS. At each step, the equations of motion (1) for both NS (superscript *N*) and PS (superscript *P*) are solved.

$$M^N \dot{Y}^N_{n+1} + R^N\left(Y^N_{n+1}\right) = L^N \Lambda_{n+1} + F^N_{n+1}$$

$$M^P \dot{Y}^P_{n+1} + R^P\left(Y^P_{n+1}\right) = L^P \Lambda_{n+1} + F^P_{n+1} \tag{1}$$

where Λ are the Lagrange multipliers, L are the Boolean matrices that localise the interfaces DoFs, M is the generalised mass matrix, F is load vector, R^N is the generalised reaction force of the numerical substructure. R^P is the generalised reaction force of the physical substructure that

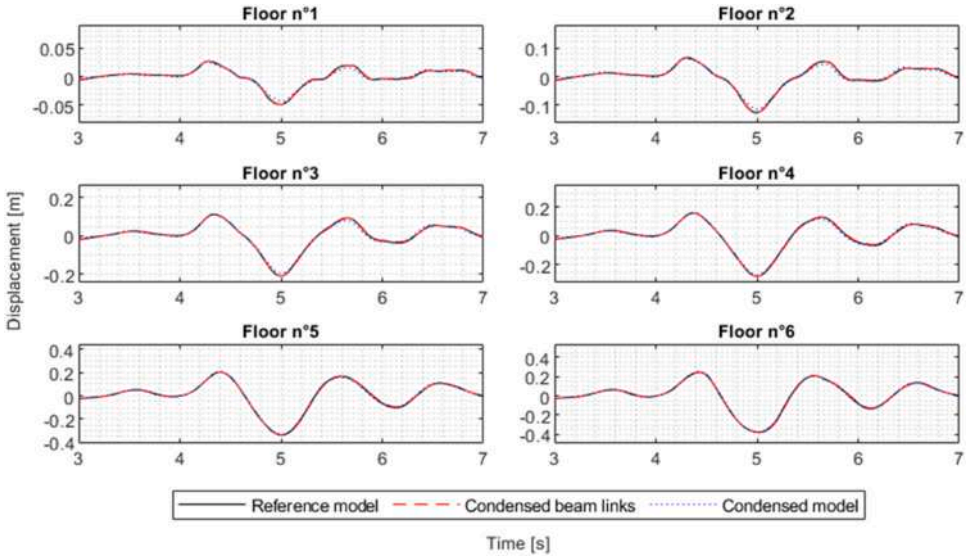

Fig. 10. Near collapse peak displacement comparison between reference and condensed models.

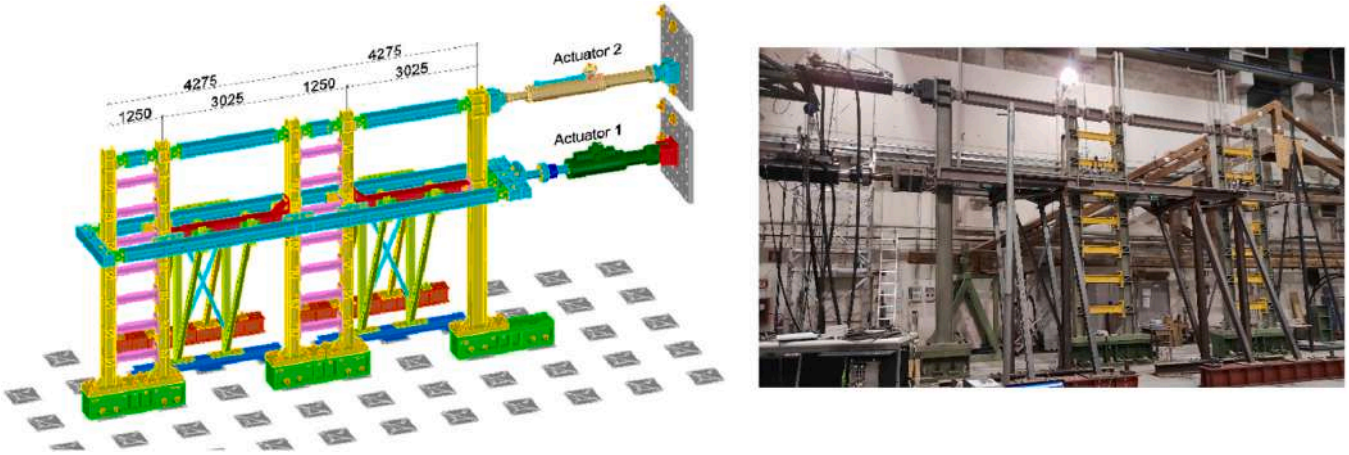

Fig. 11. Experimental test set-up.

Table 4
Mechanical properties of hot-rolled and welded profiles.

Property	S355 hot-rolled profiles		S460 welded profiles		S235 welded profiles	
	HEA 340	HEB 240	t = 16 mm	t = 10 mm	t = 8 mm	t = 5 mm
Yield strength f_y [MPa]	385	409	512	545	281	304
Ultimate strength f_u [MPa]	529	499	620	649	370	418
Elongation at failure [%]	29	29	29	25	39	30

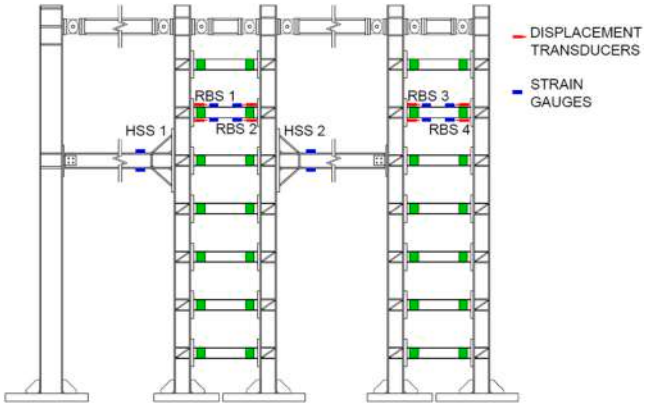

Fig. 12. Configuration of the instrumentation system for the DRLF-HSS frame.

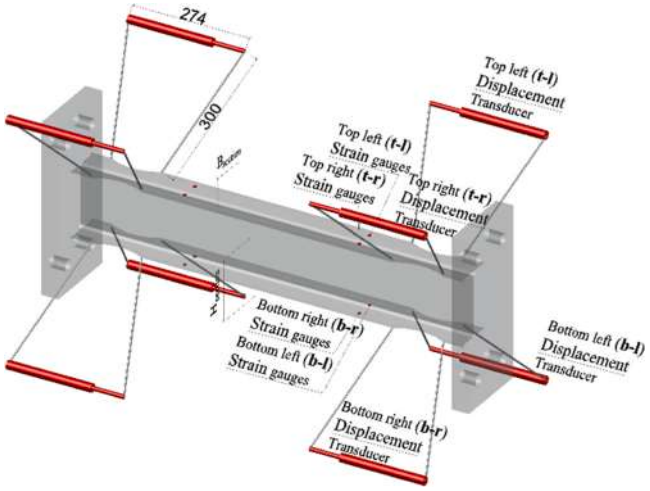

Fig. 13. Strain gauges location and displacement transducer location on the beam link.

is partially measured after the movement of actuators and forwarded to the controller. Since the equation of motion (Eq. 1) is written in state-space form, the state vector Y^N and vector R^N read, respectively:

$$Y^N = \begin{bmatrix} u^N \\ v^N \\ s^N \end{bmatrix}, \quad R^N = \begin{bmatrix} -v^N \\ r^N(u,v,s) \\ g^N(u,v,s) \end{bmatrix} \tag{2}$$

In Eq. (2), u, v and r are the displacement, velocity and restoring force vectors, whilst s is an additional state vector used to model non-linearities and $g(u,v,s)$ is the non-linear function that models the evolution of this additional state vector. Since the Bouc-Wen model [61] was implemented for modelling the evolution of the RBSs non-linear behaviour, the additional state vector s is the hysteretic displacement $z(t)$ and the differential Eq. (3) represents the non-linear function $g(v,z)$ that was implemented in the laboratory PC. The Bouc-Wen restoring force $r(t)$ is given by Eq. (4) where α is the ratio between the post-yielding and the initial elastic stiffness, and k is the initial elastic stiffness.

$$\dot{z} = \frac{[Av - v(\beta|v||z|^{n-1}z + \gamma v|z|^n)]}{\eta} \tag{3}$$

$$r(t) = \alpha k u(t) + (1-\alpha)kz(t) \tag{4}$$

In Eq. (3) A, β, γ and n are parameters that control the shape of the hysteretic loops whilst η and ν govern the main stiffness and strength degradation phenomena, respectively. In addition, the HSs were performed as pseudodynamic tests, which entailed expanding the simulation time by a constant time-scale factor λ. The method can avoid performing tests in real-time, which could not be possible given the limitations of the laboratory equipment. Consequently, the contributions of mass and damping of the physical and numerical substructure were only numerically considered. In particular, a damping ratio of 2 % was set in the numerical substructure, whereas it was set to zero for the

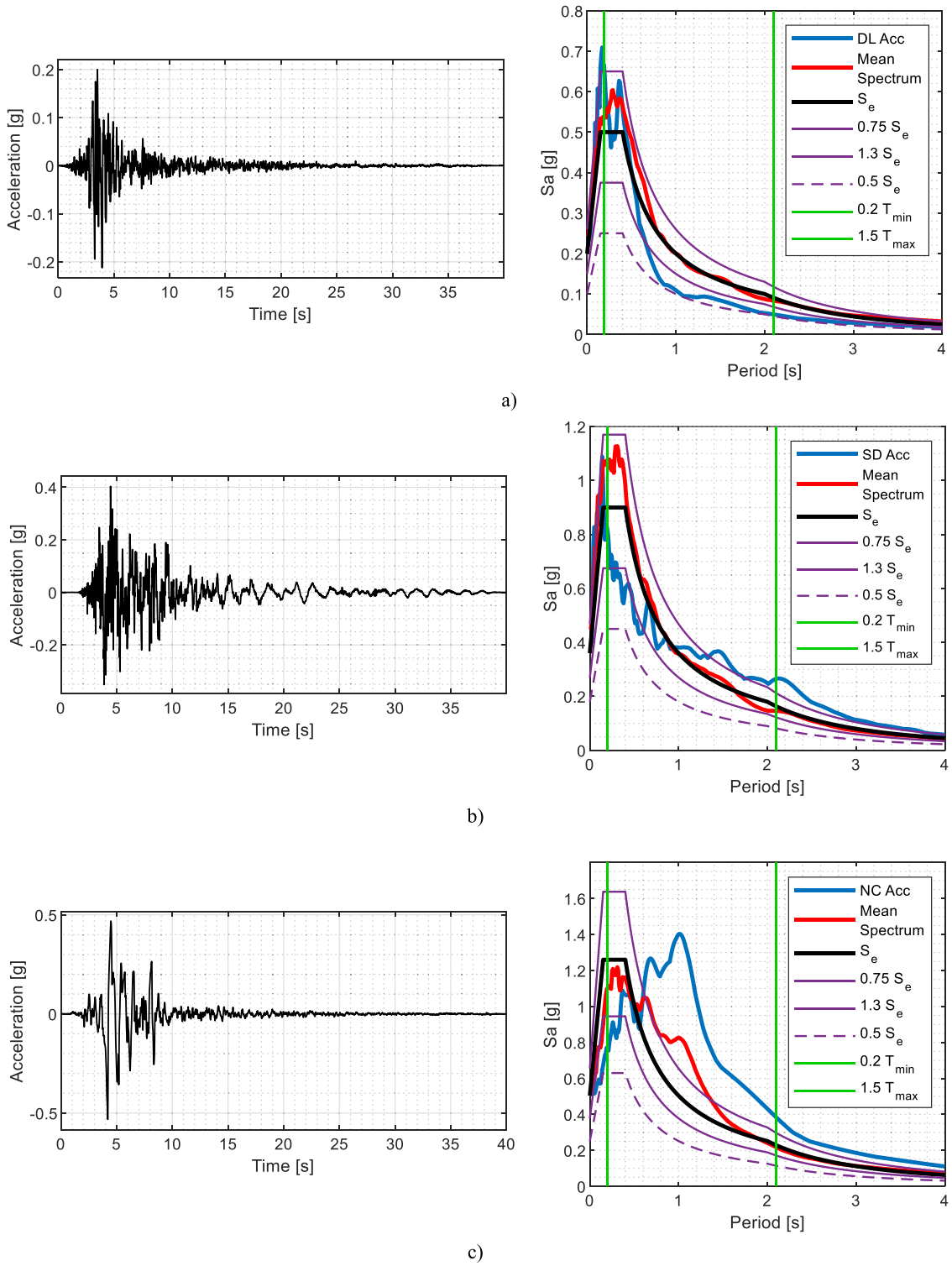

Fig. 14. Selected accelerators and spectro-compatibility: a) DL accelerogram - rsn763; b) SD accelerogram - rsn4483; c) NC accelerogram - rsn3548.

Table 5
Accelerogram main characteristics.

Database Record Number	Event	Year	Station	PGA [g]	M_w	Component	Limit state	Scaling factor
rsn763	Loma Prieta	1989	Gilroy – Galivan Coll.	0.21	6.93	East	DL	2.16
rsn4483	L'Aquila, Italy	2009	L'Aquila - Parking	0.40	6.30	East	SD	1.20
rsn3548	Loma Prieta	1989	Los Gatos - Lexington Dam	0.53	6.93	East	NC	1.20

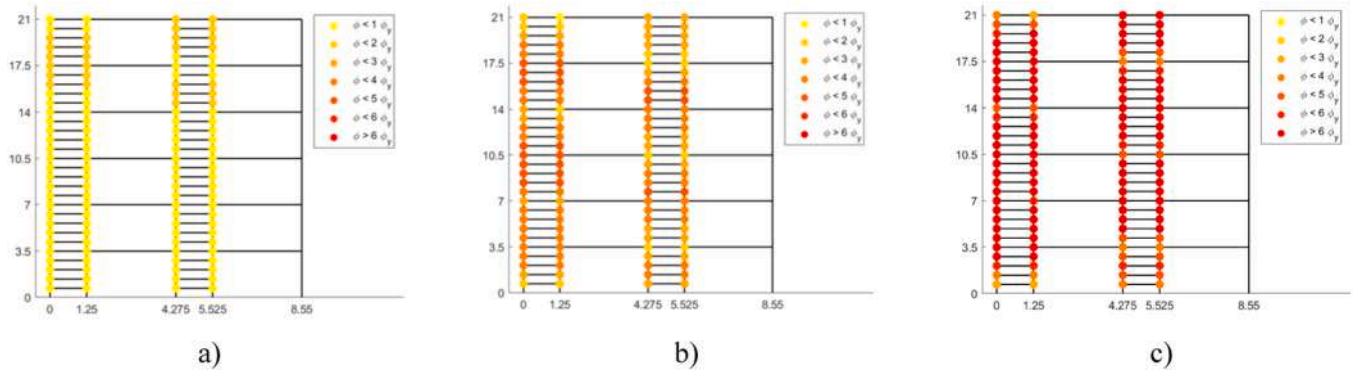

Fig. 15. Maximum RBSs rotation for the selected accelerograms at: a) DL; b) SD; c) NC limit state.

Table 6
Parameters error between monolithic and substructured frame responses. Values in %.

Parameters	DL	SD	NC
NRMSE – Bending Moment	7.43	13.40	8.17
NENERR – Bending Moment	5.37	9.52	16.85

physical part, given the inherent damping of the latter due to friction in bolted joints and other non-linear phenomena. The value of λ was varied between 50, for the test at DL limit state, and 100, for SD and NC tests.

4.2. Hybrid test configuration

The test set-up involved the use of two actuators, namely Actuator 1 and Actuator 2, located respectively at the top of the first-floor level and at the mid-height of the second floor, see Fig. 11. An axially rigid system, consisting of two beams laterally placed at the floor level, was adopted to impose the same displacement at each column, to reproduce the rigid diaphragm behaviour and to prevent the application of a significant axial force to the beam links composing the DRLF system. Furthermore, to impose the same displacement to each column, beams with high axial stiffness were placed at the level of the top actuator. Finally, a truss system was adopted to brace the frame laterally and prevent any out-of-plane instability. It is worth noting that, the availability of IPE S235 and HEB S460 profiles was scarce. For this reason, such members were made of welded cross-sections in such a way to reproduce the characteristics of the relative hot-rolled profiles as close as possible. Material testing was performed, and all the actual mechanical properties are reported in Table 4. For the S235 profiles, the material properties of the one equivalent to an IPE 160 are shown.

The configuration of the instrumentation is schematised in Fig. 12. Two beam links were fully instrumented by means of displacement transducers and strain gauges at two sections in an elastic region near the RBSs. The strain gauges were installed to estimate the bending moment, while the displacement transducers were employed to compute the rotation of the RBS. Moreover, to get an accurate measurement of the out-of-plane deformation on each beam link section, strain gauges were located at each of the four edges of the section, as depicted in Fig. 13. The displacement transducers were installed at a distance l_{bar} equal to 300 mm and oriented 45° with respect to the horizontal plane to amplify the displacements read by the instruments. Moreover, the HSS coupling beams were instrumented by means of strain gauges to estimate the bending moment.

In this respect, both the in-plane and out-of-plane curvatures were calculated by assuming plane sections, as reported in Eq. (5), where all the subscripts refer to Fig. 13 and B_{sec} is the cross-section width, whilst H_{sec} is the cross-section height.

$$\chi_y = \frac{(\varepsilon_{t,l} + \varepsilon_{t,r})/2 - (\varepsilon_{b,l} + \varepsilon_{b,r})/2}{H_{\text{sec}}}$$

$$\chi_z = \frac{(\varepsilon_{t,l} + \varepsilon_{b,l})/2 - (\varepsilon_{t,r} + \varepsilon_{b,r})/2}{B_{\text{sec}}} \tag{5}$$

An estimation of the bending moment on each instrumented section, located in the elastic range, could then be obtained by means of the

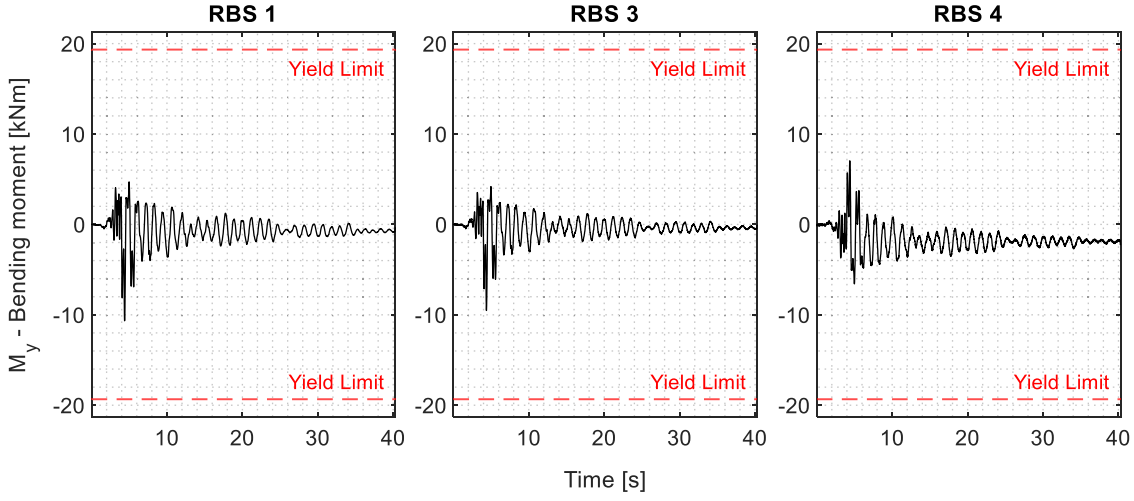

Fig. 16. DL - Bending moment time history of RBSs.

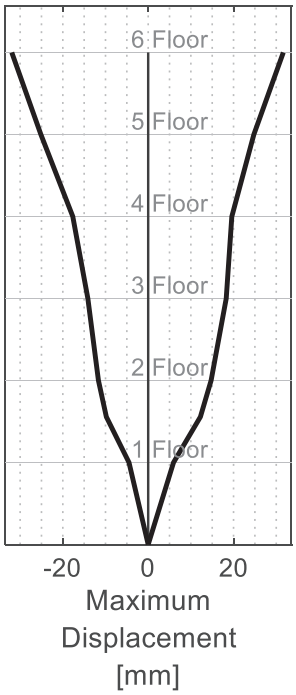

Fig. 17. DL - Maximum displacement of the six floors.

Table 7
DL – Interstorey drift ratio [%].

Floor	Absolute Maximum	Residual
1	0.17	0.0037
1-2 midpoint	0.35	0.0062
2	0.18	0.0061
3	0.34	0.0038
4	0.25	0.0038
5	0.22	0.0037
6	0.22	0.0037

elastic theory (Eq. (6)) in which I_{beam} is the modulus of inertia of the gross section and E_s is Young's steel modulus.

$$M_y = E_s I_{y,beam} \chi_y$$

$$M_z = E_s I_{z,beam} \chi_z \tag{6}$$

The bending moment along both the strong and the weak axis at the RBS could be derived by linear interpolation from the bending moments obtained in the elastic range of the beam. The rotation of the RBSs was calculated then as:

$$\varphi_y = \frac{(\Delta_{t,l} + \Delta_{t,r})/2 - (\Delta_{b,l} + \Delta_{b,r})/2}{H_{sec} + 2\cdot(l_{bar}\sqrt{2}/2)}$$

$$\varphi_z = \frac{(\Delta_{t,l} + \Delta_{b,l})/2 - (\Delta_{t,r} + \Delta_{b,r})/2}{B_{sec} + 2\cdot(l_{bar}\sqrt{2}/2)} \tag{7}$$

4.3. Test programme and ground motion selection

The seismic response of the frame was investigated by means of a series of HSs with increasing intensity of the seismic action, which corresponds to three different limit states, namely Damage Limitation (DL), Significant Damage (SD) and Near Collapse (NC). The test programme was conducted as follows:

1) Test at DL limit state. After the test, the elastic behaviour of dissipative components and the structural members was checked.
2) Test at SD limit state. After the test, the elastic behaviour of the non-dissipative structural members and inelastic behaviour of the dissipative components were checked.
3) The beam links were replaced with new ones. The self-centring capacity of the prototype building was verified and the residual interstorey drift was measured.
4) Test at NC limit state. After the test, the behaviour of structural members and dissipative components was checked.

For each limit state, a set of seven triplets of accelerograms was analysed with the aim to select the most suited ones to conduct the test. The criteria of spectral compatibility, structural performance and error minimisation between monolithic and substructured frames were considered. As illustrated in Fig. 14, for each limit state, the spectral compatibility was satisfied in accordance with the provisions of the new Eurocode 8–1C8 [67]. It is worth noting that the selected ground motion for NC limit state was a pulse-like record and did not respect the imposed limits within the range of periods indicated by the draft of the new Eurocode 8–1C8. However, Eurocode 8–1C8 allows for the use of such accelerograms; hence it was employed to obtain a structural damage substantially different from the one at the SD limit state. In Table 5, the main characteristics of the accelerograms are summarised. To evaluate the structural performance, the maximum rotation achieved by the RBSs

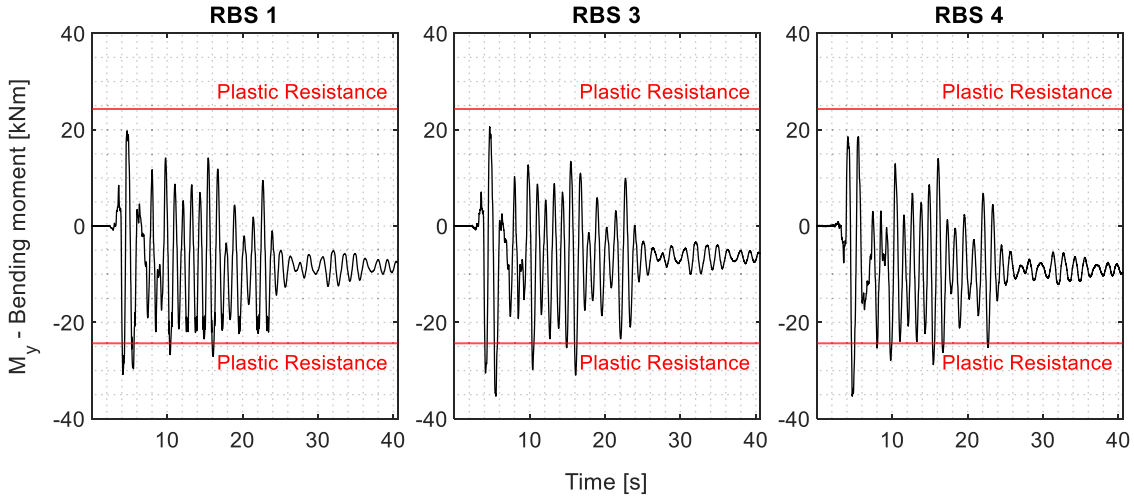

Fig. 18. SD - Bending moment time-histories of RBSs.

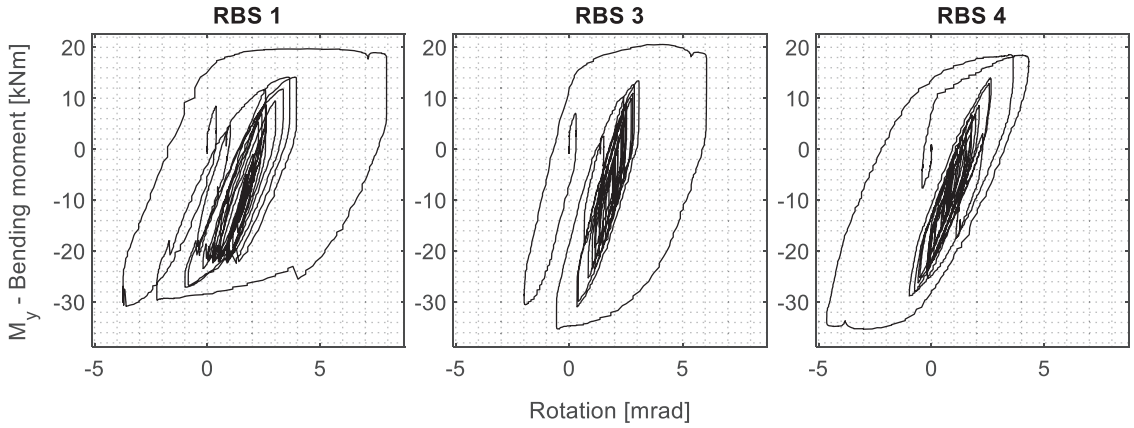

Fig. 19. SD - Moment-rotation diagrams of RBSs.

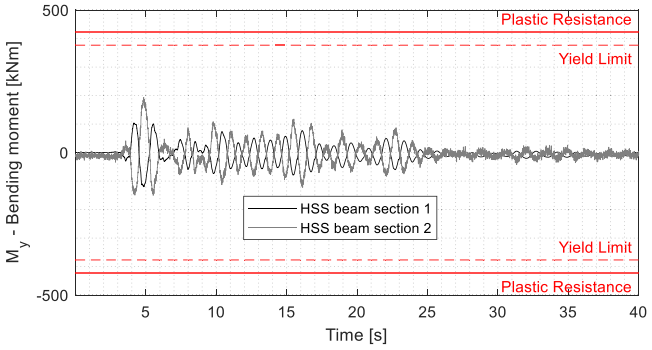

Fig. 20. SD - Bending moment time-histories at HSS fixed joints.

Table 8
Maximum displacements and forces attained during the test by the actuators.

		Actuator 1	Actuator 2
Displacement [mm]	Push	19.98	40.39
	Pull	-26.68	-54.64
Force [kN]	Push	172.68	476.38
	Pull	-226.18	-577.30

was considered. In particular, it was verified that, for the DL limit state, the rotations remained below the yield limit, i.e., 2.15 mrad, 3.19 mrad, 4.92 mrad respectively for IPE160, IPE 140 and IPE100, as shown in Fig. 15a. Moreover, it was sought that the accelerograms at the SD and NC limit states induced a uniform and diffusive inelastic behaviour in the DRLF system, as illustrated in Fig. 15b and c. It is possible to observe that at the DL limit state, the majority of the beam links remained in the elastic range, whereas at the SD and NC limit states the DRLF system exhibited large and uniformly distributed dissipation.

Finally, the consistency between the monolithic and the sub-structured response was analysed by computing the statistical indicators on the bending moment evolution of the RBSs, i.e., NENERR and NRMSE calculated as in Eq. (8).

$$\text{NRMSE} = \frac{\left\|\mathbf{x}_i - \mathbf{x}_j\right\|_2/\sqrt{N}}{\mathbf{x}_{j,\max} - \mathbf{x}_{j,\min}}$$

$$\text{NENERR} = \left|\frac{\left\|\mathbf{x}_i\right\|_2 - \left\|\mathbf{x}_j\right\|_2}{\left\|\mathbf{x}_j\right\|_2}\right| \tag{8}$$

In Eq. (8), the bending moment evolution of the two compared models is considered, i.e. the 2D substructured frame i and the 2D monolithic frame j, in which j is the dataset taken as reference. The statistical indicators described in Eq. (8) are expressed in percentages. The mean errors among all the devices for the selected accelerograms are listed in Table 6, where satisfactory outcomes are highlighted.

Table 9
SD – Interstorey drift ratio [%].

Floor	Absolute Maximum	Residual
1	0.76	0.0102
1-2 midpoint	1.50	0.0095
2	1.06	0.0103
3	1.95	0.0103
4	0.84	0.0104
5	0.73	0.0104
6	0.73	0.0104

5. Description of the results

5.1. Damage Limitation limit state

At the DL limit state, the frame behaved elastically. In fact, the maximum bending moment along the strong axis (M_y) of three representative RBSs (see Fig. 12) was lower than the elastic resisting moment, as reported in Fig. 16, that was estimated equal to 19.34 kNm, based on the reduced cross-section properties. Unfortunately, the strain gauges installed at the RBS 2 section got damaged during the erection process of the frame and could not be replaced; therefore, no accurate information could be obtained in that case.

The elastic behaviour is also confirmed by looking at the maximum displacement depicted in Fig. 17 and measured at each floor, which corresponds to a peak interstorey drift ratio (PIDR) of 0.35 %, as reported in Table 7. This value is largely lower than the conventional limit for the DL limit state of 0.7 % suggested by FEMA356 [68] for moment resisting frames. Moreover, Table 7 highlights a residual maximum interstorey drift lower than 0.01 %, which is deemed negligible.

5.2. Significant Damage limit state

As expected, at the SD limit state, the structure underwent plastic deformations, localised at the RBSs of the beam links. In particular, Fig. 18 shows the bending moment time-history of the three instrumented RBSs and it is possible to observe that the bending moment exceeded the plastic bending moment, computed as 24.34 kNm considering the actual material properties and cross-section dimensions. Fig. 19 shows the wide hysteretic cycles of the RBSs, confirming the ability of the DRLF system to dissipate a large amount of energy.

In Fig. 20, the evolution of the bending moment at end sections of the HSS coupling is depicted. It can be highlighted that the bending moment on the HSS beams is lower than the yield limit, confirming the ability of

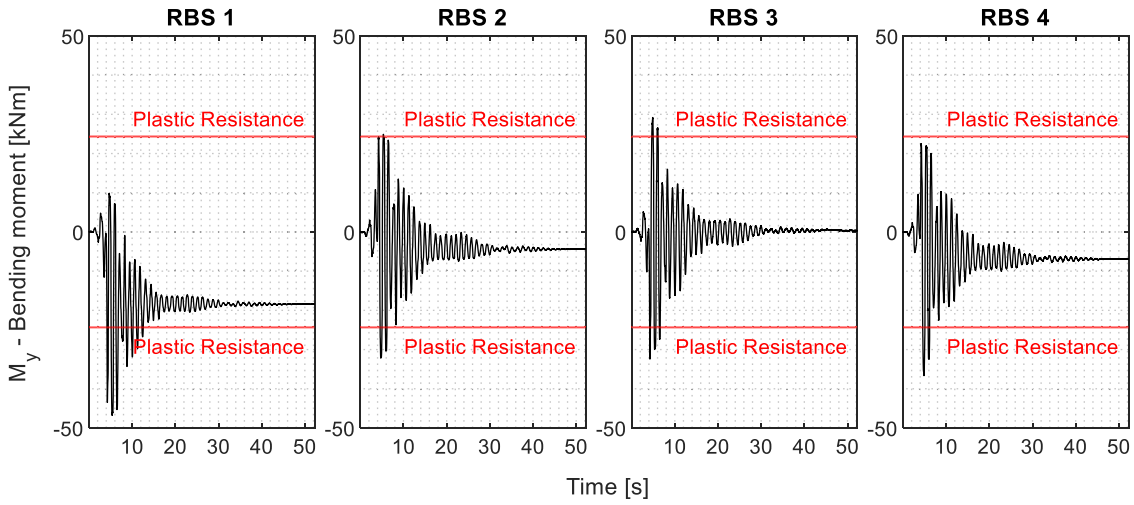

Fig. 21. NC - Bending moment time-histories of RBSs.

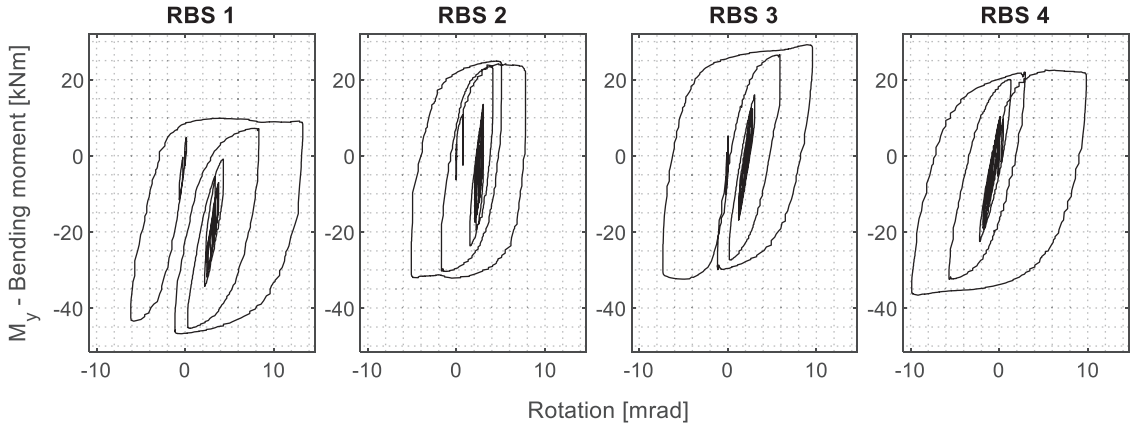

Fig. 22. NC - Moment-rotation diagrams of RBSs.

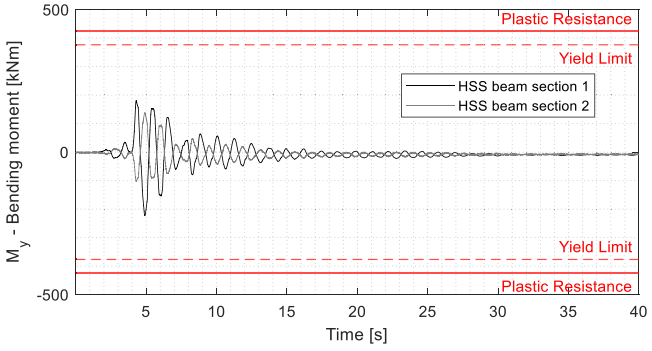

Fig. 23. NC - Bending moment time-histories at HSS fixed joints.

the DRLF devices to protect the irreplaceable elements. Finally, the maximum values of force and displacement attained during the test for the two actuators are reported in Table 8.

By computing the interstorey drift ratio (IDR), it was found that the maximum value attained during the test for the PS was 1.50 %, while for the NS was 1.95 %, as reported in Table 9. Moreover, Table 9 reports the residual interstorey drift that was equal to 0.01 %, which confirms the self-centring capability of the DRLF system coupled with HSS beams that allows the rapid replacement of the beam links in the context of enhanced structural seismic resilience.

5.3. *Near Collapse limit state*

After the replacement of the beam links, the HS at the NC limit state was performed. The frame exhibited a strong non-linear behaviour characterised by the plasticisation of the RBSs, as depicted in Fig. 21 and Fig. 22, where the bending moment time-histories of the four RBSs (see Fig. 12) are shown along with the moment-rotations diagrams.

During the ground motion the plastic bending moment was exceeded and the RBSs showed large hysteretic behaviour, with maximum rotations greater than 10 mrad. Nevertheless, besides the RBSs plasticisation, the structure remained in the elastic field. In fact, Fig. 23 shows the evolution of the bending moment at end sections of the HSS coupling beams (see Fig. 12) that is lower than the elastic bending moment.

The maximum displacement at each floor is shown in Fig. 24, whereas the peak and the residual IDR are reported in Table 10. The maximum IDR was equal to 4.14 %, which is less than the conventional limit of 5 % for the NC limit state given by FEMA356 [68]. Nevertheless, the residual IDR value is significantly low, 0.03 %, thereby confirming the structure self-centring capability.

Regarding the out-of-plane behaviour of the beam links, Fig. 25 depicts the bending moment time-history along the weak axis (M_z) of the RBSs. Notably, the maximum value attained, which is 2.07 kNm, is only little lower than the plastic resistance of the RBS, specifically 2.79 kNm, resulting in a working rate of 74 % in the worst-case scenario. Therefore, particularly at the NC limit state, the out-of-plane bending moment may

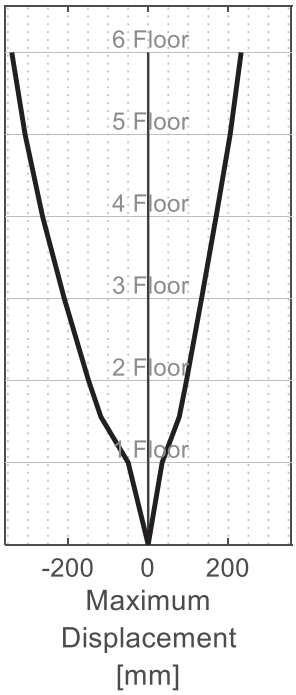

Fig. 24. NC - Maximum displacement of the six floors.

Table 10
NC – Interstorey drift ratio [%].

Floor	Absolute Maximum	Residual
1	1.42	0.0313
1-2 midpoint	3.50	0.0314
2	2.32	0.0310
3	4.14	0.0312
4	1.68	0.0314
5	1.37	0.0310
6	1.37	0.0310

influence the resistance and the overall response of the beam links. Moreover, small residual bending moment was exhibited by the RBSs due to the global residual plastic deformation.

5.4. Repairability considerations

The experimental campaign results on the DRLF systems combined with HSS coupling beams indicated minimal residual interstorey drift ratio after the SD and NC limit states, with maximum values of 0.01 % and 0.03 % recorded at the end of the tests. This finding enhances the ease of replacement of the damaged beam links after a significant seismic event and highlights the self-centring capability. The residual interstorey drifts can be compared with the threshold value of 0.2 %, which is the FEMA P58–1 [69] limit value to ensure that no structural realignment is necessary. Moreover, the measured values are also lower than 0.5 % [70], which is conventionally assumed as a permissible residual interstorey drift ratio to ensure the building repairability. Furthermore, the experimental results were highly encouraging as they emphasised the effortless nature of such replacements. In fact, hydraulic jacks were used to securely substitute dissipative devices following an earthquake. This technique guarantees minimal disruption to the structural integrity of the building, while allowing the equipment to be replaced quickly and effectively. Notably, the replacement time for first-floor devices was particularly short: about 6 man/h. This level of efficiency not only minimises possible business downtime but also increases the overall seismic resilience of the structure. Moreover, the aforementioned value can easily be used to determine the repair time of an entire building.

5.5. Experimental versus numerical results

This section presents the comparison between the experimental results and the outcomes of non-linear numerical analyses performed on the 3D model developed in OpenSees. For brevity, only the limit states that induced inelastic behaviour in the DRLF system were considered. Compared with the test data at the SD and the NC limit states, the FE model accurately captures the overall seismic response parameters, e.g. base shear and top floor displacement. Specifically, the differences between the actual and predicted peak displacements or peak forces are mostly within 20 %, as reported in Table 11. The history over time of the response parameters for the three limit states are depicted in Fig. 26 and Fig. 27, respectively.

6. Conclusions

The paper provides comprehensive information about the experimental campaign carried out at the University of Trento on a full-scale steel frame equipped with a dissipative system, namely Dissipative Replaceable Link Frame (DRLF) with the exploitation of HSS coupling

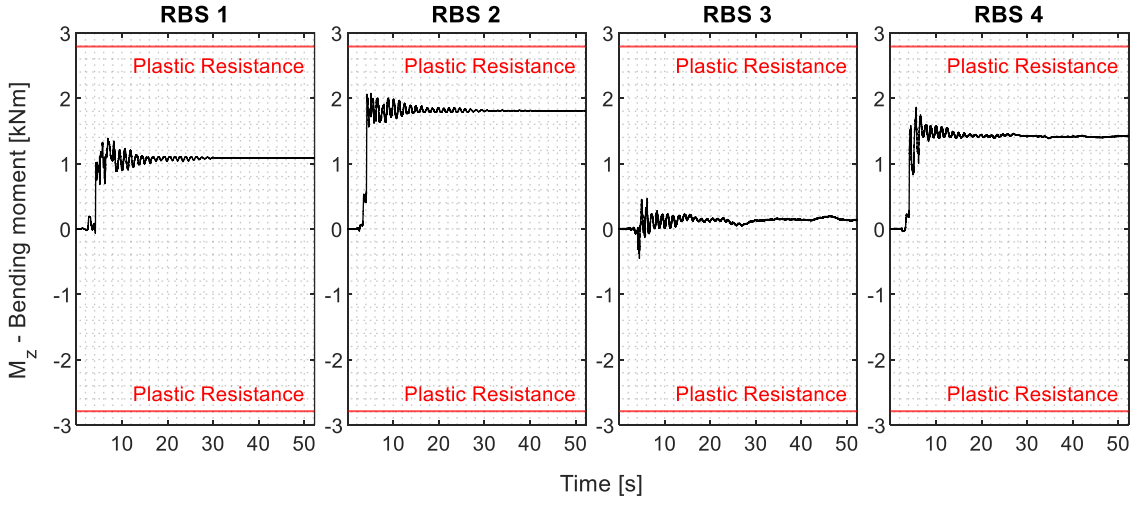

Fig. 25. NC - Bending moment time-histories of RBSs along the weak axis.

Table 11
Experimental vs numerical comparison.

		SD			NC		
		Test	FE	Error [%]	Test	FE	Error [%]
Base Shear [kN]	Pull	492.84	408.44	17 %	711.6	578.13	19 %
	Push	604.12	608.42	1 %	1008	765.3	24 %
Top Floor Displacement [m]	Pull	0.148	0.172	16 %	0.222	0.241	9 %
	Push	0.174	0.207	19 %	0.340	0.371	9 %

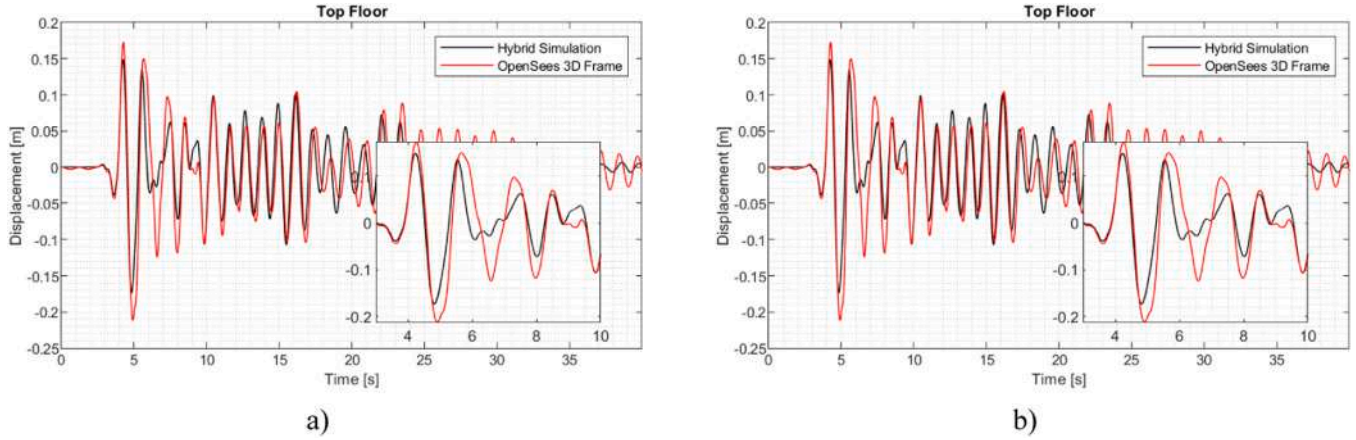

Fig. 26. Top floor displacement comparison: a) Significant damage; b) Near Collapse.

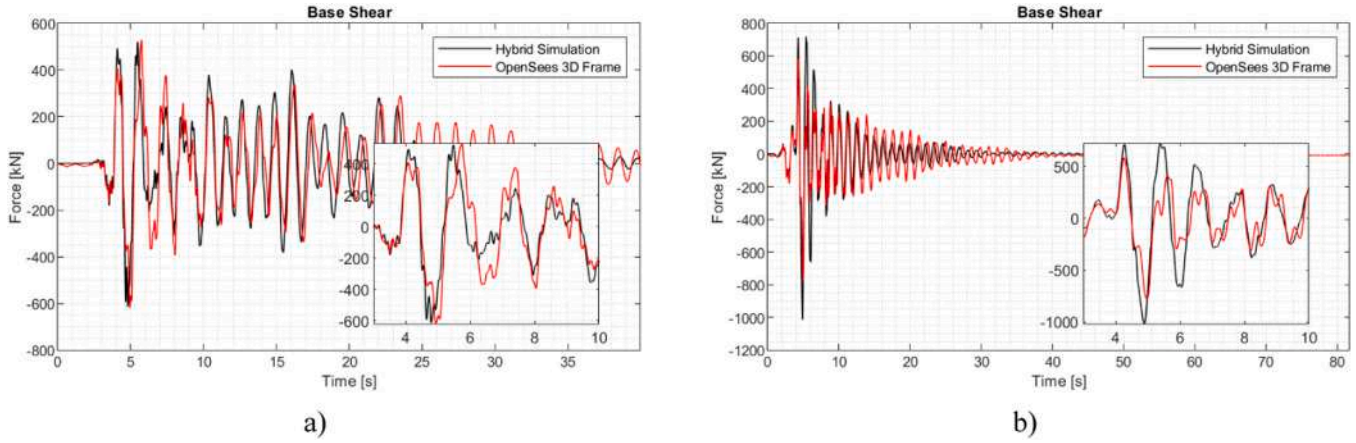

Fig. 27. Base shear comparison: a) Significant damage; b) Near Collapse.

beams. The seismic response of the whole frame under increasing seismic intensity was investigated by means of HSs. HS allowed for physically testing only the ground floor and numerically simulating the remainder of the structure, i.e. the five floors above. The tests were conducted at three different limit states, i.e. Damage Limitation, Significant Damage and Near Collapse limit state. The following main conclusions could be drawn:

- At the DL limit state, the design assumptions of elastic behaviour of the structure were satisfied.
- At the SD limit state, the beam links of the DRLF system underwent large and favourable energy dissipation. The residual interstorey drift ratio was negligible, i.e. 0.01 %, mainly due to the coupling HSS beams remaining within the elastic range, enhancing structural stiffness and self-centring capabilities. This low drift ratio made replacing beam links easy, taking only about 6 man-hours, demonstrating significant advantages for improved structural resilience.
- At the NC limit state, no damage was detected on the irreplaceable parts, e.g. the HSS coupling beams and columns, whilst the reduced beam sections of the beam links underwent significant and favourable inelastic dissipative behaviour. Also, the residual interstorey drift ratio at the NC was negligible, highlighting the self-centring capabilities.

Finally, this work has demonstrated the benefits of using HSS coupling beams in combination with the DRLF system to increase the frame stiffness and its self-centring capabilities without consuming space on the facades, as is the case with bracing systems. Furthermore, thanks to its inherent overstrength, the higher steel grade ensured the plasticisation of the dissipative elements. Future perspectives include the employment of the calibrated components for numerical

applications, e.g., Incremental Dynamic Analyses and seismic fragility curves.

CRediT authorship contribution statement

Giulia Giuliani: Writing – original draft, Validation, Software, Methodology, Data curation. **Roberto Andreotti:** Writing – review & editing, Software, Methodology, Data curation. **Alessio Bonelli:** Writing – review & editing, Supervision, Methodology. **Nicola Tondini:** Writing – review & editing, Supervision, Methodology, Funding acquisition, Conceptualization.

Declaration of Competing Interest

The authors declare that they have no known competing financial interests or personal relationships that could have appeared to influence the work reported in this paper.

Data availability

Data will be made available on request.

Acknowledgements

This work was carried out with a financial grant from the Research Fund for Coal and Steel of the European Union, within the DISSIPABLE project: "Fully dissipative and easily repairable devices for resilient buildings with composite steel-concrete structures", Grant No. 800699-RFCS-2017. The results reflect only the author's view and the Commission is not responsible for any use that may be made of the information it contains. The authors also acknowledge the Italian Ministry of Education, Universities and Research (MUR), in the framework of the project DICAM-EXC (Departments of Excellence 2023-2027, grant L232/2016).

References

[1] CEN (European Committee for Standardization). Eurocode 8: design of structures for earthquake resistance - Part 1: General rules, seismic actions and rules for buildings. 2005.
[2] Engineers AS of C. Minimum design loads and associated criteria for buildings and other structures. American Society of Civil Engineers; 2017.
[3] Construction AI of S. Seismic provisions for structural steel buildings. American Institute of Steel Construction,; 1997.
[4] Plumier A. New idea for safe structures in seismic zones. IABSE Symp -Mixed Struct Incl N Mater 1990. https://doi.org/10.5169/SEALS-46518.
[5] Iwankiw NR, Carter CJ. The dogbone: a new idea to chew on. Mod Steel Constr 1996;36(4):18–23.
[6] Francavilla AB, Latour M, Piluso V, Rizzano G. Design of full-strength full-ductility extended end-plate beam-to-column joints. J Constr Steel Res 2018;148:77–96.
[7] Tartaglia R, D'Aniello M, Zimbru M. Experimental and numerical study on the T-Stub behaviour with preloaded bolts under large deformations. In: Structures. Elsevier; 2020. p. 2137–55.
[8] Latour M, Rizzano G. A theoretical model for predicting the rotational capacity of steel base joints. J Constr Steel Res 2013;91:89–99.
[9] Rodas PT, Zareian F, Kanvinde A. Hysteretic model for exposed column–base connections. J Struct Eng 2016;142:04016137.
[10] Elnashai A, Elghazouli A. Seismic behaviour of semi-rigid steel frames. J Constr Steel Res 1994;29:149–74.
[11] Chen S-J, Yeh CH, Chu JM. Ductile steel beam-to-column connections for seismic resistance. J Struct Eng 1996;122:1292–9. https://doi.org/10.1061/(ASCE)0733-9445(1996)122:11(1292).
[12] Pucinotti R, Tondini N, Zanon G, Bursi OS. Tests and model calibration of high-strength steel tubular beam-to-column and column-base composite joints for moment-resisting structures: high-strength steel tubular beam-to-column and column-base composite joints. Earthq Eng Struct Dyn 2015;44:1471–93. https://doi.org/10.1002/eqe.2547.
[13] Montuori R, Nastri E, Piluso V, Troisi M. Influence of connection typology on seismic response of MR-Frames with and without 'set-backs. Earthq Eng Struct Dyn 2017;46:5–25.
[14] Tondini N, Zanon G, Pucinotti R, Di Filippo R, Bursi OS. Seismic performance and fragility functions of a 3D steel-concrete composite structure made of high-strength steel. Eng Struct 2018;174:373–83. https://doi.org/10.1016/j.engstruct.2018.07.026.
[15] MacRae GA, Clifton GC, Mackinven H, Mago N, Butterworth J, Pampanin S. The sliding hinge joint moment connection. Bull N Z Soc Earthq Eng 2010;43:202–12.
[16] Borzouie J, Chase J, MacRae G, Rodgers G, Clifton G. Spectral assessment of the effects of base flexibility on seismic demands of a structure. Adv Civ Eng 2016;2016:1–8.
[17] Piluso V, Pisapia A, Nastri E, Montuori R. Ultimate resistance and rotation capacity of low yielding high hardening aluminium alloy beams under non-uniform bending. Thin-Walled Struct 2019;135:123–36.
[18] Latour M, Piluso V, Rizzano G. Experimental analysis of innovative dissipative bolted double split tee beam-to-column connections. Steel Constr 2011;4:53–64. https://doi.org/10.1002/stco.201110009.
[19] Freddi F, Dimopoulos CA, Karavasilis TL. Experimental evaluation of a rocking damage-free steel column base with friction devices. J Struct Eng 2020;146:04020217.
[20] Francavilla AB, Latour M, Piluso V, Rizzano G. Design criteria for beam-to-column connections equipped with friction devices. J Constr Steel Res 2020;172:106240. https://doi.org/10.1016/j.jcsr.2020.106240.
[21] Di Benedetto S, Francavilla AB, Latour M, Piluso V, Rizzano G. Experimental response of a large-scale two-storey steel building equipped with low-yielding friction joints. Soil Dyn Earthq Eng 2022;152:107022. https://doi.org/10.1016/j.soildyn.2021.107022.
[22] Chan RW, Albermani F. Experimental study of steel slit damper for passive energy dissipation. Eng Struct 2008;30:1058–66. https://doi.org/10.1016/j.engstruct.2007.07.005.
[23] Oh S-H, Kim Y-J, Ryu H-S. Seismic performance of steel structures with slit dampers. Eng Struct 2009;31:1997–2008. https://doi.org/10.1016/j.engstruct.2009.03.003.
[24] Alehashem SMS, Keyhani A, Pourmohammad H. Behavior and performance of structures equipped with ADAS & TADAS dampers (a comparison with conventional structures). 14th World Conf Earthq Eng 2008;12:17.
[25] Fortney PJ, Shahrooz BM, Rassati GA. Large-Scale Testing of a Replaceable "Fuse" Steel Coupling Beam. J Struct Eng 2007;133:1801–7. https://doi.org/10.1061/(ASCE)0733-9445(2007)133:12(1801).
[26] Dusicka P, Iwai R. Development of linked column frame system for seismic lateral loads. Struct. Eng. Res. Front. Long Beach, California, United States: American Society of Civil Engineers,; 2007. p. 1–13. https://doi.org/10.1061/40944(249)63.
[27] Lopes A, Dusicka P, Berman J. Linked column framing system analyses toward experimental validation. Struct. Congr, 2012. Chicago, Illinois, United States: American Society of Civil Engineers,; 2012. p. 1598–609. https://doi.org/10.1061/9780784412367.142.
[28] Malakoutian M, Berman JW, Dusicka P. Seismic response evaluation of the linked column frame system. Earthq Eng Struct Dyn 2013;42:795–814. https://doi.org/10.1002/eqe.2245.
[29] Li F, Zhao B, Li Y, Lü T, Wang G. Experimental and numerical studies on the hysteretic behavior of linked column frame with uplifted column feet. J Constr Steel Res 2022;197:107441. https://doi.org/10.1016/j.jcsr.2022.107441.
[30] Montuori R, Nastri E, Piluso V, Pisapia A. Design procedure for failure mode control of linked column frames. Eng Struct 2023;296:116937. https://doi.org/10.1016/j.engstruct.2023.116937.
[31] Ezoddin A, Kheyroddin A, Gholhaki M. Experimental and numerical investigation on the seismic retrofit of RC frames with linked column frame systems. J Build Eng 2021;44:102956. https://doi.org/10.1016/j.jobe.2021.102956.
[32] Fang C, Qiu C, Wang W, Alam MS. Self-centering structures against earthquakes: a critical review. J Earthq Eng 2023:1–36.
[33] Hu S, Wang W, Alam MS, Ke K. Life-cycle benefits estimation of self-centering building structures. Eng Struct 2023;284:115982.
[34] Elettore E, Freddi F, Latour M, Rizzano G. Parametric study and finite element analysis of self-centring steel column bases with different structural properties. J Constr Steel Res 2022;199:107628.
[35] Plumier A, Doneux C, Castiglioni CA. Two innovations for earthquake-resistant design: the INERD project: final report. Publications Office; 2006.
[36] Castiglioni, Dougka CA, Kalteziotis G, Karydakis Ph D, Calado L, Kanyilmaz A, et al. Dissipative devices for seismic-resistant steel frames (Fuseis). LU: Publications Office; 2013.
[37] Vayas I. Innovative Dissipative (INERD) Pin Connections for Seismic Resistant Braced Frames n.d.:12.
[38] Dougka G, Dimakogianni D, Vayas I. Innovative energy dissipation systems (FUSEIS 1-1) — Experimental analysis. J Constr Steel Res 2014;96:69–80. https://doi.org/10.1016/j.jcsr.2014.01.003.
[39] Dimakogianni D, Dougka G, Vayas I. Seismic behavior of frames with innovative energy dissipation systems (FUSEIS 1-1). Earthq Struct 2014;6:561–80. https://doi.org/10.12989/EAS.2014.6.5.561.
[40] Kanyilmaz A, Muhaxheri M, Castiglioni CA. Influence of repairable bolted dissipative beam splices (structural fuses) on reducing the seismic vulnerability of steel-concrete composite frames. Soil Dyn Earthq Eng 2019;119:281–98. https://doi.org/10.1016/j.soildyn.2019.01.007.
[41] Kanyilmaz A, Kondratenko A, Castiglioni CA, Calado L, Proença JM, Mouzakis H, et al. Fully dissipative and easily repairable components for resilient buildings with composite steel-concrete structures. Eur Comm Proj Number 2022:800699.
[42] Andreotti R, Giuliani G, Tondini N. Experimental analysis of a full-scale steel frame with replaceable dissipative connections. J Constr Steel Res 2023;208:108036. https://doi.org/10.1016/j.jcsr.2023.108036.
[43] Andreotti R, Giuliani G, Tondini N, Bursi OS. Hybrid simulation of a partial-strength steel–concrete composite moment-resisting frame endowed with hysteretic replaceable beam splices. Earthq Eng Struct Dyn 2023;52:51–70. https://doi.org/10.1002/eqe.3744.

[44] Giuliani G, Andreotti R, Tondini N. Hybrid simulation of a steel frame with Dissipative Replaceable Link Frames. Bull Earthq Eng 2024. https://doi.org/10.1007/s10518-024-01907-y.
[45] Pinkawa M., Bartsch H., Schaffrath S., Hoffmeister B., Feldmann M. Seismic design of steel frames with fuseis beam link energy dissipation systems, Rhodes Island, Greece; 2017, p. 878–90. ⟨https://doi.org/10.7712/120117.5463.18111⟩.
[46] Pinkawa M., Vulcu C., Hoffmeister B., Feldmann M. Optimization of dissipative replaceable link frames by elastic high strength steel coupling beams, Athens, Greece; 2020, p. 3127–3143. https://doi.org/10.47964/1120.9256.20314.
[47] Vulcu C, Pinkawa M, Hoffmeister B. Comparison of the seismic performance of conventional moment resisting frames and innovative dissipative replaceable link frames. Timis, Rom 2022:8.
[48] Hu F, Shi G, Shi Y. Experimental study on seismic behavior of high strength steel frames: Global response. Eng Struct 2017;131:163–79. https://doi.org/10.1016/j.engstruct.2016.11.013.
[49] Lian M, Su M. Seismic testing and numerical analysis of Y-shaped eccentrically braced frame made of high-strength steel. Struct Des Tall Spec Build 2018;27:e1455. https://doi.org/10.1002/tal.1455.
[50] Chen Y, Ke K. Seismic performance of high-strength-steel frame equipped with sacrificial beams of non-compact sections in energy dissipation bays. Thin-Walled Struct 2019;139:169–85. https://doi.org/10.1016/j.tws.2019.02.035.
[51] Nakashima M. Hybrid simulation: an early history. Earthq Eng Struct Dyn 2020;49:949–62. https://doi.org/10.1002/eqe.3274.
[52] Abbiati G, Bursi OS, Caperan P, Di Sarno L, Molina FJ, Paolacci F, et al. Hybrid simulation of a multi-span RC viaduct with plain bars and sliding bearings. Earthq Eng Struct Dyn 2015;44:2221–40. https://doi.org/10.1002/eqe.2580.
[53] Del Carpio Ramos M, Mosqueda G, Hashemi MJ. Large-scale hybrid simulation of a steel moment frame building structure through collapse. J Struct Eng 2016;142:04015086. https://doi.org/10.1061/(ASCE)ST.1943-541X.0001328.
[54] Di Benedetto S, Francavilla AB, Latour M, Ferrante Cavallaro G, Piluso V, Rizzano G. Pseudo-dynamic testing of a full-scale two-storey steel building with RBS connections. Eng Struct 2020;212:110494. https://doi.org/10.1016/j.engstruct.2020.110494.
[55] Vayas I. Innovative anti-seismic devices and systems: INNOSEIS Project RFCS-02-2015. 1st ed. Zürich: ECCS; 2017.
[56] CEN (European Committee for Standardization). Eurocode 8: Design of structures for earthquake resistance - Part 3: Assessment and retrofitting of buildings. 2005.
[57] CSI C and SInc. SAP2000 Integrated Software for Structural Analysis and Design 2019.
[58] Mattei F, Giuliani G, Andreotti R, Caprili S, Tondini N. Experimental and numerical assessment of a steel frame equipped with Dissipative Replaceable Bracing Connections. Procedia Struct Integr 2023;44:1204–11. https://doi.org/10.1016/j.prostr.2023.01.155.
[59] CEN (European Committee for Standardization). Eurocode 3: Design of steel structures - Part 1–1: General rules and rules for buildings. 2005.
[60] McKenna F, Fenves G, Scott M. University of California Berkeley. Open: Open Syst Earthq Eng Simul 2006.
[61] Wen Y-K. Method for random vibration of hysteretic systems. J Eng Mech Div 1976;102:249–63. https://doi.org/10.1061/JMCEA3.0002106.
[62] Smith M. ABAQUS/Standard User's Manual; 2009.
[63] Giuliani G, Andreotti R, Tondini N, Bonelli A. Experimental investigation of steel frames equipped with dissipative replaceable links. Ce/Pap 2022;5:714–9. https://doi.org/10.1002/cepa.1811.
[64] Flores F, Charney F, Lopez-Garcia D. The influence of gravity column continuity on the seismic performance of special steel moment frame structures. J Constr Steel Res 2016;118:217–30. https://doi.org/10.1016/j.jcsr.2015.11.010.
[65] Pastor M, Binda M, Harčarik T. Modal Assurance Criterion. Procedia Eng 2012;48:543–8. https://doi.org/10.1016/j.proeng.2012.09.551.
[66] Abbiati G, Lanese I, Cazzador E, Bursi OS, Pavese A. A computational framework for fast-time hybrid simulation based on partitioned time integration and state-space modeling. Struct Control Health Monit 2019;26. https://doi.org/10.1002/stc.2419.
[67] CEN (European Committee for Standardization). Eurocode 8: Design of structures for earthquake resistance - Part 1: general rules, seismic actions and rules for buildings. Working draft; 2018.
[68] FEDERAL EMERGENCY. Prestandard and commentary for the seismic rehabilitation of buildings - FEMA 356. vol. 356; 2000.
[69] Applied Technology Council. Seismic performance assessment of buildings. Redwood City, CA; 2012.
[70] McCormick J, Aburano H, Ikenaga M, Nakashima M. Permissible residual deformation levels for building structures considering both safety and human elements. Beijing: Seismological Press; 2008. p. 12–7.